ANALYSIS OF HEAT INPUT EFFECTS IN PASSIVE THERMOGRAPHIC NDE

David A. Tossell
Materials Science and Engineering Department
434 Dougherty Engineering Building
University of Tennessee
Knoxville, TN 37996-2200

INTRODUCTION

The use of digital imaging techniques for analysing and enhancing IR video frames in thermographic NDE [1-6] allows some improvement in resolution of surface temperature contrast. Of equal importance, however, to the magnitude and longevity of the generated contrast is the magnitude and length of the function governing the input heating rate and source impedance [7]. In thermogaphic testing the limiting factor is usually the maximum temperature rise (or drop) over a given time span that the heated (cooled) face of the sample can be subjected to without damage occuring. In this study single step and profiled radiative heat pulses have been assessed numerically and experimentally and compared to contact heating (as with a hot liquid in a flexible bag). The detrimental effects of convective and radiative surface heat losses have been examined and their significance to the testing of low and high diffusivity materials assessed. All results presented here are for the two-sided testing configuration although, in principle, the results are applicable to single sided testing also.

NUMERICAL MODEL

The numerical part of this study was carried out using the thermal analysis software package ITAS (Interactive Thermal Analysis System [8]) available for the IBM PC. This is essentially a numerical difference analyser suitable for solving lumper parameter problems which are governed by diffusion type equations. The problem is descibed in terms of nodes, conductors, heat sources and constant temperature boundaries. In thermogaphic NDE it is essential to model in three dimensions because one or two dimensional models do not fully allow for heat flow around the edges of a defect. For the most part studies of this nature are carried out on mainframe computers in which case three dimensional models are easily constructed by using many nodes in a block, the defect being represented by one or more impaired conductors. However in the case of a small computer this is impracticable since the program would take unnacceptably long times to run. To overcome this problem the model shown schematically in Figure 1 was constructed to represent a segment of

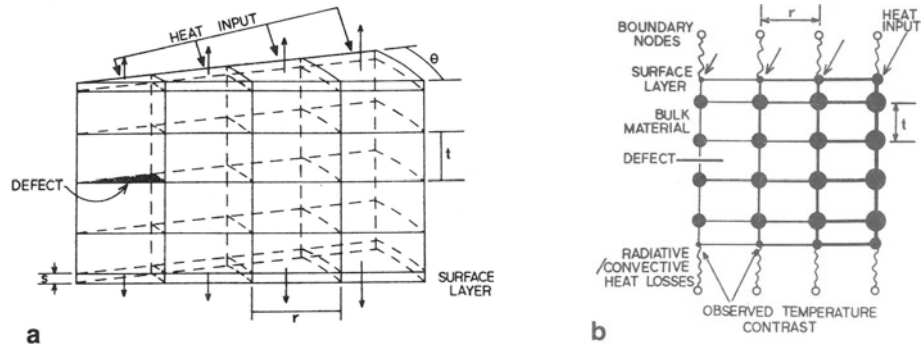

Fig. 1. Schematic (a) and nodal (b) diagrams of the finite difference thermal model.

isotropic material, the sizes of the nodes and thicknesses of the connecting lines representing the magnitude of the capacitances and conductances respectively. This necessitates that nodal capacitances and conductances differ from row to row and column to column but these calculations are easily relegated to a simple computational program. The input nodal and conductance values may be calculated from

$$\text{Nodal capacitance} = A\ t\ C\ \rho \qquad (1)$$

Where A = through thickness area of node = $0.5\ \theta\ (r_i^2 - r_{i-1}^2)$, this is merely the difference in area between two sectors.

t = thickness of the node.
C = specific heat capacity of material.
ρ = density of material.

$$\text{Connector conductance} = kA/\ l \qquad (2)$$

Where A = area of conductor in the direction of heat flow.
k = thermal conductivity of the material.
l = length of conductor in direction of heat flow.

Inspection of the model will reveal that all nodes and conductors are represented exactly except those conductors in the radial direction. For these conductors the conducting area is taken as an average of the areas at each end of the connector. This approximation is minimised by making the segment thin, i.e. small θ (here $\theta = 0.2$ radians). This two dimensional model now represents accurately a segment of a three dimensional cylinder containing a circular flat two dimensional defect. To give more realistic surface temperatures a thin layer of low capacitance nodes were included on the front and back surfaces, this avoids the effect of a large capacity surface node averaging the "surface" temperature over a considerable depth. The defect to diameter ratio is therefore $(2t + s)/\ 2r$. The defect was assigned a conductivity of zero throughout this study. Heat inputs were represented by direct input to one set of surface nodes, each individual nodal input being suitably adjusted to take account of the differing areas to give a constant heating rate per unit area. Contact heating was simulated by connecting the front surface nodes to boundary nodes of fixed higher temperature by conductors of length half the thickness of the surface layer. Surface temperature contrasts due to the defect were taken between the surface node directly

above the defect and the surface edge node furthest from it. Results were checked by varying the program control constants; convergence criterion, time step and iterations per step so as to guard against the anomalous results that can occur in numerical network programs. Although this mesh is somewhat coarse all numerical results were verified experimentally. Using this compact model run times were reduced from several hours (for a rectangular block of 175 nodes) to several minutes.

EXPERIMENTAL

The experimental apparatus is shown schematically in Figure 2 and is composed of a Hughes thermal imaging system plus a radiant heater and shutter. The radiant heater was mounted on a movable support on an optical bench and kept at a fixed temperature. The input heat flux for several positions of the heater on the bench was determined by observing the front face temperature rise of a sample over a period of time with the shutter open. In this way the input heat flux incident on the sample was calibrated as a function of the position of the heater on the bench. All experiments were carried out using epoxy resin slabs of dimensions 30 x 25 mm and 3mm thick, each containing a mid-plane defect of nominal diameter 7mm. This gives a depth to diameter ratio of 0.21 which gives rise to

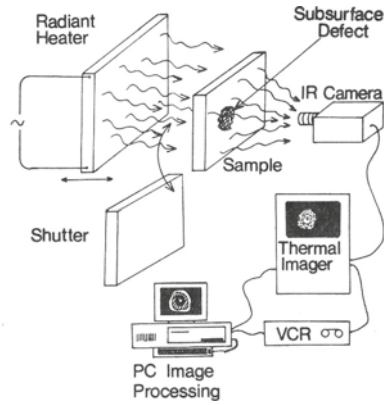

Fig. 2. Experimental apparatus.

surface temperature contrasts large enough to distinguish between the various input heating pulses. To minimise emmissivity effects the samples were painted with carbon black and for the present purposes the maximum allowed front face temperature rise was limited to 20°C. Epoxy resin was chosen as the sample material because it has a very low thermal diffusivity (α = 0.09 x10^{-6} $m^2 s^{-1}$), therefore transient temperature fields persist for relatively long periods of time. This aids recording and, more importantly, the effects of convective and radiative heat loss on the surface temperature contrast to be clearly seen. In a high diffusivity material (i.e. metals) the temperature transients are brief and thermal losses very small.

Contact heating experiments were carried out using hot water in a flexible bag which was pressed against the front face of the sample.

RESULTS

Single Radiative Pulse Heat Input

The most common form of heat input function used in transient video thermography is the single step, i.e. one flux level for a fixed period of time which raises the front face temperature to some limiting value then switches off. For a fully insulated slab the relationship between the duration and magnitude of such a pulse can be expressed [9]

$$Q = \frac{1}{\left(\tau + \frac{1}{3} - \sum_{n=1}^{\infty} \frac{2}{(n\pi)^2} \exp(-(n\pi)^2\tau)\right)} \qquad (3)$$

Where Q = Dimensionless input heat flux $ql/k\Delta T$
τ = Dimensionless time $\propto t/l^2$
and q is input heat flux W/m^2
l is slab thickness m
k is thermal conductivity $W/m^{\circ}C$
ΔT is front face temperature rise $^{\circ}C$
$\propto$ is thermal diffusivity $m^2 s^{-1}$
t is time s

In Figure 3 curve i shows the calculated maximum back surface temperature contrast that is generated for a perfectly insulated sample for a range of Q, the duration of each pulse being determined from Eq.3. For comparison the maximum calculated and experimental temperature contrasts generated via contact heating are also shown. Curve i is dimensionless and can be used to determine the optimum pulse parameters for any defective isotropic homogeneous slab of similar d/ϕ ratio given appropriate material constants. For example, the pulse that gives highest temperature contrast is $Q = 1.425$ and $= 0.41$, for a 3mm thick slab this translates into 1400 W/m^2 for 38 seconds for epoxy resin and 2.2 MW/m^2 for 0.036 seconds for aluminium.

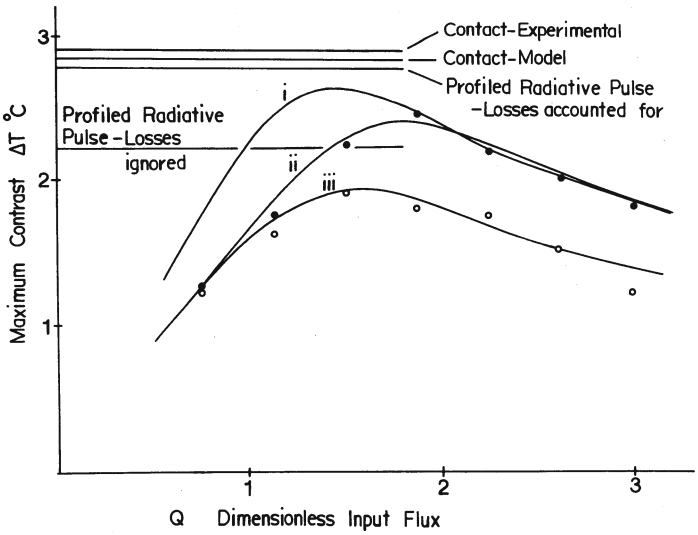

Fig. 3. Maximum temperature contrast (ΔT) versus input heating flux for single step pulses. (i) Fully insulated specimen, (ii) lossy specimen using same heating pulses as for (i), (iii) lossy specimen with losses accounted for. For comparison the maximum contrasts for contact and profiled radiative pulse heating are also shown.

The data points on curve iii in Figure 3 are experimentally observed contrasts using the same pulse parameters as curve i for a resin slab in ambient air (25°C). It is apparent that the surface heat losses severely inhibit the observed contrast. Fitting a curve to these data the convective and radiative losses from the sample can be deduced. This allows a new longer pulse length for each input flux to be calculated such that the front surface temperature rise reaches the limiting value precisely (except at low input flux levels where the losses are such that steady state conditions are reached below this limit). The calculated curve and experimental values of contrast for the extended pulses are also shown in Figure 3, curve ii. Accounting for heat losses does not restore the original contrast, this is because the initial penetration of heat into the sample is always reduced by front surface losses. Also it is difficult to apply this result generally since the losses are predominantly a function of the surface rather than material constants, thus while curve i is truly dimensionless curve ii is unique to the present sample material and dimensions.

Figure 4 compares the form of the single step pulses that give maximum contrast for each curve in Figure 3. ii is shorter than i since there is less heat loss in a shorter time period. iii takes account of all heat losses and is therefore larger and longer. The modification of the pulse from i to iii is governed by material thermal constants, absolute temperature and surface heat transfer and is therefore unique to any given test.

Putting thermal constants for aluminium into the model and using the convective and radiative conductances for surface losses deduced from the resin sample it was found that curves i and iii superimpose. In general, surface heat losses to air and radiation from high diffusivity materials can be ignored.

Profiled Radiative Heat Pulse Input

In general the largest surface temperature constants are generated when the front face temperature of the sample is raised quickly to, and maintained at, a fixed value. This is the reason high contrasts are obtained using contact heating, such as with a hot liquid in a flexible bag. In addition, this heating method is the ideal for all defect to diameter ratios (d/ϕ) unlike single step pulses which are dependent on d/ϕ. For contact heating the dimensionless heat flux, Q, across the front surface of the slab can be expressed

$$Q = \sum_{n=-\infty}^{+\infty} \exp\left(-(n\pi)^2\tau\right) \qquad \text{(Fully insulated slab)} \qquad (4)$$

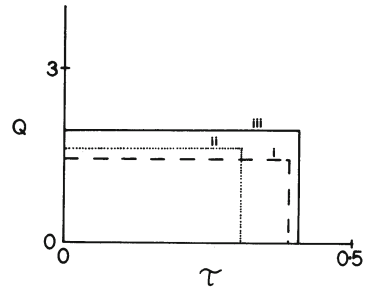

Fig. 4. Comparison of the three single step pulses that give maximum temperature contrast for the curves of Figure 3.

$$Q = \sum_{n=0}^{\infty} 2 \exp\left(-\left((2n+1)\frac{\pi}{2}\right)^2 \tau\right) \qquad \text{(Heatsunk back surface)} \qquad (5)$$

Symbols defined as for Eq.3. These two expressions are shown graphically as curves 1 and 2 in Figure 5. Again high diffusivity materials (i.e. metals) approximate well and surface heat losses can be ignored. Curve 3 in Figure 5 has been calculated using the nodal model for contact heating of a 3mm thick resin sample in ambient air at 25°C and, as might be expected, lies between curves 1 and 2. Taking account of convective, and convective and radiative losses give rise to curves 4 and 5. Attention is drawn to

i) The increased value of Q between 0 and 0.5τ. The difference between curves 4 and 5 and curve 1 can be directly attributed to heat loss from the front surface. Contrast is diminished if the front surface losses are ignored.

ii) The magnitude of the radiative losses. Frequently, in practice, convective losses are accounted for and radiative losses ignored since the latter are difficult to model. Comparison of curves 1,4 and 5 reveal that the losses due to radiation are about 1/2 of those due to convection. This is for an experiment which raises the front surface temperature from 25°C to 45°C. At higher temperatures radiative losses will be more significant.

Figure 6 shows two multistep curves derived from curves 1 and 5 in Figure 5. These were implemented experimentally by calibrating the input heat flux from a radiative heater at various points on an an optical bench. The profiles of Figure 5 were then mimicked by moving the heater away from the sample at the appropriate times. The maximum contrasts obtained using these profiles are shown in Figure 1 for comparison with the single step pulse cases. Also shown are the maximum experimental and calculated contrasts generated by contact heating using a flexible bag containing water 20°C hotter than the initial temperature of the specimen. The profile based on curve 5 gives a maximum contrast that is close to that for contact heating. However the result for the profile derived from curve 1 is poor since this treats the slab as perfectly insulated and is inferior to the best single pulse that accounts for heat loss.

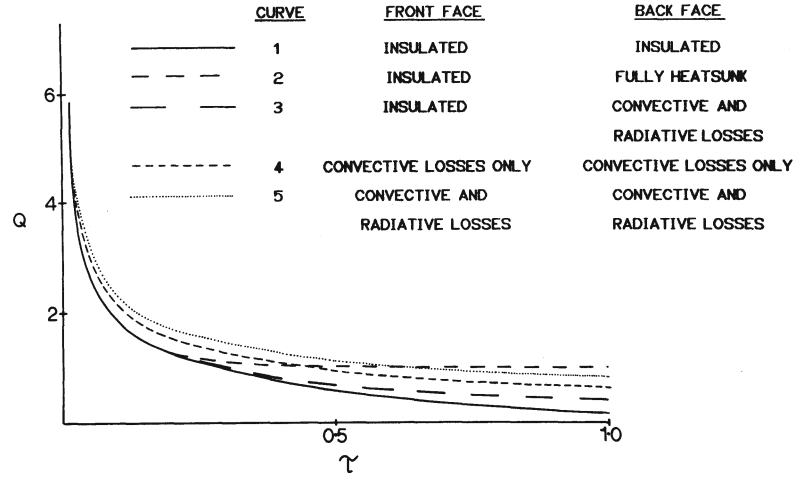

Fig. 5. Heating profiles for a variety of specimen conditions.

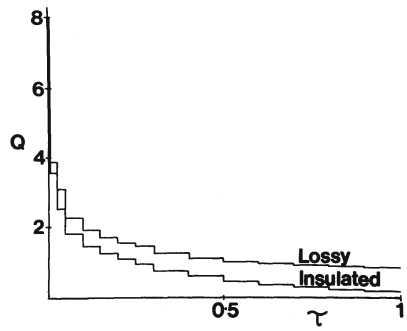

Fig. 6. Multistep heating profiles that mimic curves 1 and 5 in Figure 5.

Figure 7 shows temperature contrasts for a variety of profiles as a function of time. It can be seen that even the best single step pulse falls some way short of contact heating both in terms of magnitude and longevity of the surface temperature contrast. Indeed the best single step pulse can be thought of as a compromise between a high initial heating rate, which gives maximum contrast, and a long low heating rate, which sustains the contrast over a long period. The profiled radiative input compares well with that for contact heating both in terms of maximum contrast and longevity.

Many thermographic techniques utilise periodically modulated heat inputs, usually a pulsed or chopped laser beam. For high frequencies and high diffusivity materials the heat losses can be ignored. However for low diffusivity materials the period of the modulation can be large enough such that heat losses become significant. Figure 8 shows a suggested modification in the modulating profile that may give significant

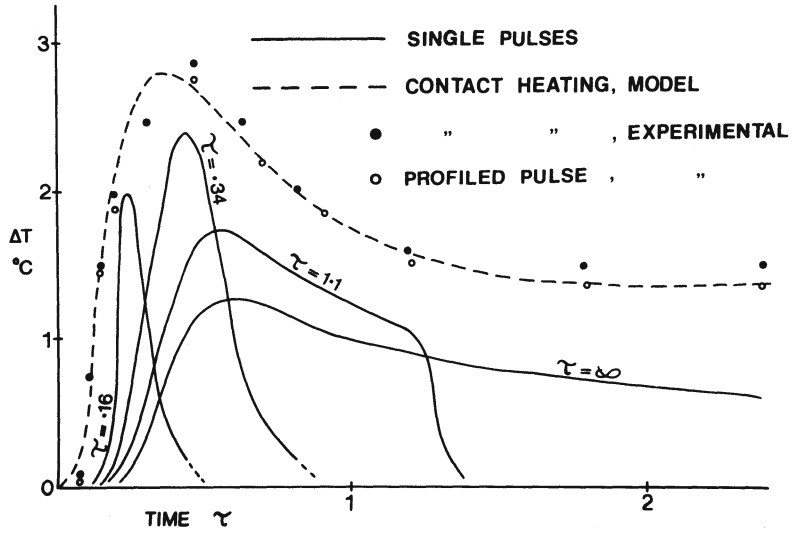

Fig. 7. Temperature contrast as a function of time for all forms of heat input examined. Single step curves correspond to inputs that account for heat loss. Note that the profiled radiative pulse and contact heating give rise to near identical contrast curves.

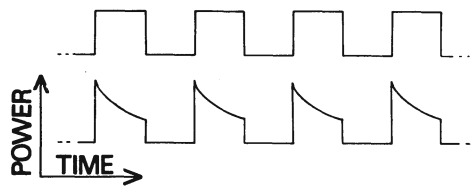

Fig. 8. Suggested modification of input heating cycle for cases where the period of the modulated wave is large.

improvement in the observed contrasts. To calculate the profile all that is required is that the heat losses be characterised and inserted into a one dimensional thermal diffusion model. In practice the profile could be generated by replacing a dark/bright chopper with a circular optical filter with the required smoothly varying transmission characteristics in a circumferential direction. By rotating this in the path of the laser beam the desired modulation could be produced.

CONCLUSIONS

i) In general heat losses can be ignored for high (metals) but not low diffusivity materials (plastics, composites).

ii) For low diffusivity materials input heating profiles must take account of radiative losses to maximise temperature contrast.

iii) For single step heat input the theoretical maximum contrast attainable for a perfectly insulated sample cannot be recovered by modifying the input to account for heat loss from the front surface.

iv) Profiled radiative heating fluxes can be derived that fully account for heat loss and compare well with contact heating.

ACKNOWLEDGEMENT

The author thanks Mr S.A.Stiner and Mr R.L.Johnson for technical assistance.

REFERENCES

1. W.N.Reynolds and G.M.Wells, Brit.J.NDT 26 40 (1984).
2. S.F.Burch, J.T.Burton, and S.J.Cocking, Brit.J.NDT 26 36 (1984)
3. J.W.Milne and W.N.Reynolds, SPIE 590 293 (1985)
4. P.Cielo, R.Lewak, and D.Balageas, SPIE 581 47 (1986)
5. J.J.Allport and S.L.McHugh, in Review of Progress in Quantitative NDE, edited by D.O.Thompson and D.E.Chimenti (Plenum Press, New York, 1988), Vol 7A, pp 253-262
6. W.P.Winfree, C.S.Welch, and P.H.James, this issue.
7. C.S. Welch, in Review of Progress in Quantitative NDE, edited by D.O.Thompson and D.E.Chimenti (Plenum Press, New York, 1988), Vol 7A, pp 279-285
8. Interactive Thermal Analysis System, R.F.Warriner Associates, 3838 Carson Street, Suite 300, Torrence, CA 90503, USA
9. H.S.Carslaw and J.C.Jaeger, Conduction of Heat in Solids (Oxford Press, London, 1959)